coatings

MDPI

Article

Investigation of the Effect of Additional Zirconium Diboride (ZrB_2) in Spherical Graphite Cast Iron on Mechanical Properties

Rifat Yakut [1,*] and Ramazan Ortakaya [2]

[1] Department of Energy Systems Engineering, Faculty of Technology, Batman University, Batman 72000, Türkiye

[2] Department of Automotive Engineering, Batman University, Batman 72000, Türkiye; r.ortakaya63@gmail.com

* Correspondence: rifat.yakut@batman.edu.tr

Abstract: Steering gearbox bodies, which are produced from spheroidal graphite cast iron, experience wear and gaps over time since they operate under load. It is important to strengthen steering gearbox bodies to avoid this. In this study, a steering gearbox body was produced from a spheroidal graphite cast iron material with zirconium diboride at varying rates (0%, 0.227%, 0.455%, and 1.364%). Samples of the material were prepared according to established standards for hardness, compressive strength, and wear resistance tests. The mechanical properties of test samples with and without zirconium diboride (hardness, compressive strength, and wear resistance) were compared. Sample C showed the highest hardness measurement of 243 HB after adding 0.455% zirconium diboride. As the rate of addition increased, the values obtained from the hardness measurement test also increased. Sample C had the highest compressive value of 1438 MPa, with a 0.455% addition rate. It was found that the compressive strength values also increased as the addition rate increased. Wear tests were conducted to analyse wear volume, wear rate, and friction coefficients. A scanning electron microscope (SEM) device was utilised to identify wear mechanisms on the worn surfaces of the samples. Per the results of this study, wear volume values were found to increase with the load value.

Keywords: steering gear box body; spheroidal graphite cast iron (SGCI); zirconium diboride (ZrB_2)

check for updates

Citation: Yakut, R.; Ortakaya, R. Investigation of the Effect of Additional Zirconium Diboride (ZrB_2) in Spherical Graphite Cast Iron on Mechanical Properties. *Coatings* **2023**, *13*, 1385. https://doi.org/10.3390/coatings13081385

Academic Editor: Chi Ma

Received: 17 July 2023
Revised: 1 August 2023
Accepted: 4 August 2023
Published: 7 August 2023

1. Introduction

Spheroidal graphite cast iron, which is also known as ductile cast iron, is characterised by spheroidal graphite containing flake graphite, unlike grey cast iron. Spherical graphite results in higher strength and superior toughness and ductility in comparison to grey cast iron of a similar composition [1]. Due to its operational properties and competitive production costs compared to other ferrous alloys, cast irons can be cast in sizes from a few millimetres to several tens of meters and in masses from a few grams to tons [2]. Iron-based metals (such as cast iron and steel) are significant commercially available materials. Although steel came to the fore at the beginning of the industrial revolution, the use of cast iron, which can compete with steel in terms of mechanical properties and can be produced more cost-effectively with technological developments, has begun to increase in many areas. Cast irons are Fe–C alloys that contain at least 2.1% C and 1%–3% Si in their chemical content [3]. Cast iron is widely used in buildings (e.g., water pipes) and the automotive (machines, engines, and exhaust manifolds) and wind power industries due to its combination of good casting properties and high mechanical properties [4]. Cast iron has many common advantages, such as excellent castability, high fatigue strength, high thermal conductivity, high vibration damping, hardness, corrosion resistance, easy machinability, wear resistance, strength, and toughness in combination [5–12]. Since cast iron is produced close to the final desired shape, even complex-shaped parts do not require additional processing and production costs are reasonable [13–15]. Spheroidal graphite cast iron, which is used in plenty of structural applications in the automotive industry, is used as a steering gearbox body material [16]. Spheroidal graphite cast iron has many advantages, such as high tensile strength and high ductility. It is also used in gear wheels, pistons, bearing caps, crankshafts, camshafts, crankshafts, camshafts, axle housings, differential carriers, pump bodies, steering bodies, and suspension arms owing to its high wear resistance, high quality in the automotive industry, and its reasonable production costs [16–18]. Spheroidal graphite cast iron has greater strength and ductility than grey cast iron [17]. Mechanical parts which are made of cast iron are generally exposed to high loads and friction. Therefore, a long service life and good performance are critical [19,20]. In general, cast iron is a self-lubricating metal-based composite material [21]. The tribological properties of cast iron are highly dependent on the state of the graphite content (size, shape, and distribution of graphite) and shear conditions [22]. Wear and damage occur with metal parts sliding against each other over time, making the machines inoperable [23].

Wear and gaps occur as the ball and ball bearings in steering gearboxes work under constant load. These gaps and wear and cause steering gearboxes to produce a lot of noise during operation. It is necessary to increase the strength of the steering gearbox bodies to prevent such abrasions. When the literature was examined, it was observed that there were not sufficient studies on adding ZrB_2, which has many superior properties, to spheroidal graphite cast iron and its effect. In this study, the aim was to increase the strength values of steering gear box bodies made of spheroidal graphite cast iron by adding zirconium diboride (ZrB_2) at different rates (sample A: 0%; sample B: 0.227%; sample C: 0.455%; and sample D: 1.364%). These produced samples' compressive strength, hardness, and wear treatment were investigated. In the wear tests, the samples were tested in a pin-on-disc wear test device per the standards under normal atmospheric and dry ambient conditions. An AISI 316 stainless steel ball with a 6 mm diameter was used as an abrasive. Tests were conducted under loads of 5 N, 8 N, 10 N, and 15 N at a sliding speed of 219.9 mm/s and a total sliding distance of 500 m. During the test, data were collected by measuring the friction coefficient values. Moreover, the effects of load changes on the wear treatment of spheroidal graphite cast iron with different amounts of ZrB_2 were investigated.

2. Materials and Methods

2.1. Material Production

Sample materials used in the experiments were produced in the Hema Automotive Systems Inc. Iron Casting Factory. Spheroidal graphite cast iron samples A (no additive), B, C, and D were melted in a metal melting furnace. The samples, whose chemical compositions are illustrated in Table 1, were poured into sand moulds separately at 1410 °C at the casting crucible temperature. Compressive strength, hardness, microstructure, and wear analyses of the produced spheroidal graphite cast iron samples were investigated. The spheroidal graphite cast iron was produced according to the ASTM A 536 standard [24,25].

Table 1. Chemical compositions of samples (wt.%).

No	C	Si	Mn	P	S	Cr	Cu	Sn	Mg	Al	Ti	ZrB_2
A	3.78	2.44	0.33	0.0034	0.0022	0.08	0.03	0.039	0.06	0.001	0.033	-
B	3.57	2.71	0.35	0.0126	0.0161	0.133	0.0872	0.0435	0.0442	0.008	0.0066	0.227
C	3.55	2.82	0.391	0.0245	0.0202	0.146	0.0986	0.0563	0.0381	0.0073	0.0167	0.455
D	3.5	2.81	0.346	0.014	0.015	0.133	0.0783	0.0452	0.051	0.007	0.0082	1.364

Nanografi Nano Technology (Türkiye) supplied the ZrB_2 additive material which was used in this study. ZrB_2 has a high melting temperature (3245 °C), high hardness (23 GPa), high strength (337–398 MPa), moderate fracture toughness (3.5 MPa $m^{1/2}$), and retains mechanical performance at elevated temperatures (1600 °C) in the air [26–28].

2.2. Preparation of Test Samples

Spheroidal graphite cast iron samples were removed from the sand moulds at room temperature after casting. From the samples removed from the sand moulds, hardness samples with dimensions of 12 mm × 32 mm × 45 mm were prepared for the A (no additive), B, C, and D ratios for hardness tests. Measurements were taken from at least 5 points from different regions on the surface of each sample, and the average hardness values of these measurements was determined. For the compressive tests, 12 cylindrical specimens of Ø10 mm × 16 mm were prepared, three from each addition ratio. The compressive ratio is determined using the ho/do formula, which was determined to be 1.6 in this study. For wear tests, samples with dimensions of 12 mm × 32 mm × 45 mm were prepared for each addition ratio. The surfaces of these prepared samples that were to be subjected to the wear test were polished before the wear test. Samples with dimensions of 15 mm × 15 mm × 15 mm were prepared for metallography processes. These samples were cut with a Metcon Metacut 250 precision cutting device. In addition, the prepared samples were primarily sanded with 120, 240, 400, 800, and 1200 mesh sandpapers. Sanding and polishing processes of the cast samples were made, and the samples were ready for microstructure examinations.

3. Results and Discussion

Karadeniz et al. found the hardness value of GGG-60 which was produced without adding inoculant to be 220.4 HB [29]. Hardness test measurements were determined according to the literature. The averages of the measurement results were retrieved and compared with those of the previous studies on spheroidal graphite cast iron. As a result of the comparisons, it appeared that the results obtained were compatible with the hardness measurement results in the literature. In the hardness measurement tests, which were performed with the Ernst AT250DR brand Brinell hardness measurement tester, the lowest measurement was for the A sample, with an average of 234 HB. The average hardness value increased in the B sample with 0.227% ZrB_2 added and was determined to be 239 HB. The C sample with 0.455% ZrB_2 added increased depending on the increase in the addition rate, and the average hardness value was measured as 243 HB. In the D sample with 1.364% ZrB_2 added, there was no significant increase in the hardness value despite the increase in addition rate. It was observed that its hardness value averaged 242 HB, with a slight decrease compared to the D sample. This is because ductile cast iron materials vary depending on their chemical composition and solidification cooling rates [16]. When the hardness test results were examined, the highest hardness value average was determined in the C sample with 0.455% ZrB_2 addition. The Brinell hardness measurement values of the samples, depending on the addition rates, are illustrated in Figure 1. Hardness measurements were carried out randomly from the sample surface.

Compressive tests were carried out in accordance with the literature because the steering gearbox that was examined in this study is not exposed to tensile stress and serves as a bearing for the gears on it. In this study, all tests were carried out under the same conditions to compare the compressive test specimens. When the compressive test results were compared with those of the literature after the experiment, it was observed that the results were in accordance with those from the literature. In the compressive tests performed according to the ASTM E9 standard [30] on the Zwick Roell Z600 universal tester, the average compressive strength of sample A was found to be 1223 MPa. The compressive strength values are expected to increase as the ZrB_2 addition rates increase. It was determined that there was an increase in the compressive strength (average of 1378 MPa) as the addition rate increased in sample B with 0.227% ZrB_2 added. In sample C with 0.455% ZrB_2 added, as the addition rate increased, an increase in the compressive strength (average of 1438 MPa) was observed in accordance with the expectation. In sample D with 1.364% ZrB_2 added, there was no increase in the compressive strength (average of 1276 MPa) despite the increase in the addition rate. The increase in the amount of spherical graphite affects the ferrite/perlite ratio in the microstructure. As this amount increases, the perlite ratio decreases, and with the effect of this decrease, the ductility increases while the strength value decreases [30–32]. The highest compressive strength was observed in sample C, with 0.455% ZrB_2 added. Compressive strength measurement values of the samples, depending on the addition rates, are illustrated in Figure 2.

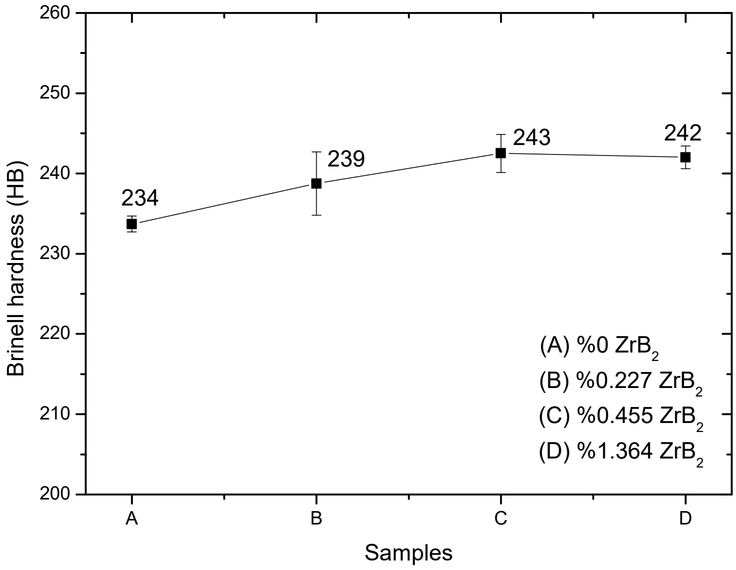

Figure 1. Brinell hardness measurement values.

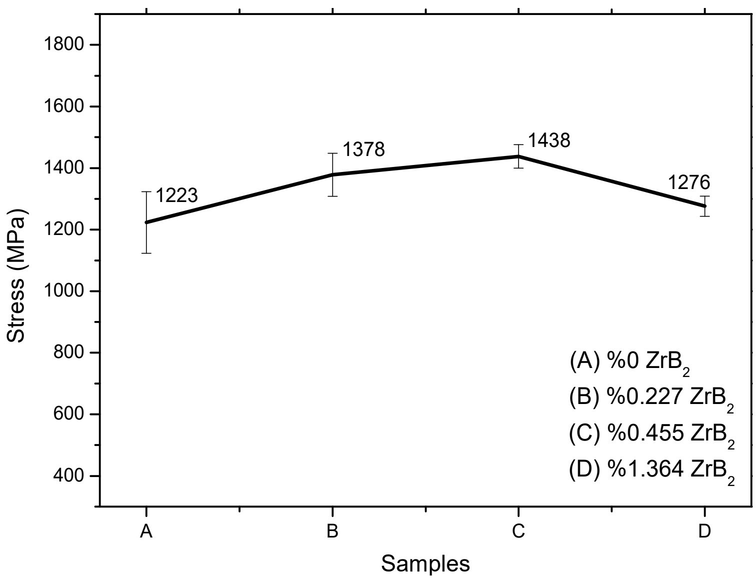

Figure 2. Compressive strength measurement values.

When the stress–strain graphs for the compressive tests were examined, it was observed that although the curves were similar, there were differences at the highest stress points. With the effect of the stresses formed in the applied compressive loads, fracture damages (Figure 3) occurred in the materials. When the damage aspects were examined, it was observed that the fractures occurred at an angle of ~45°. Stress–strain plots for the compressive strength tests are illustrated in Figure 4.

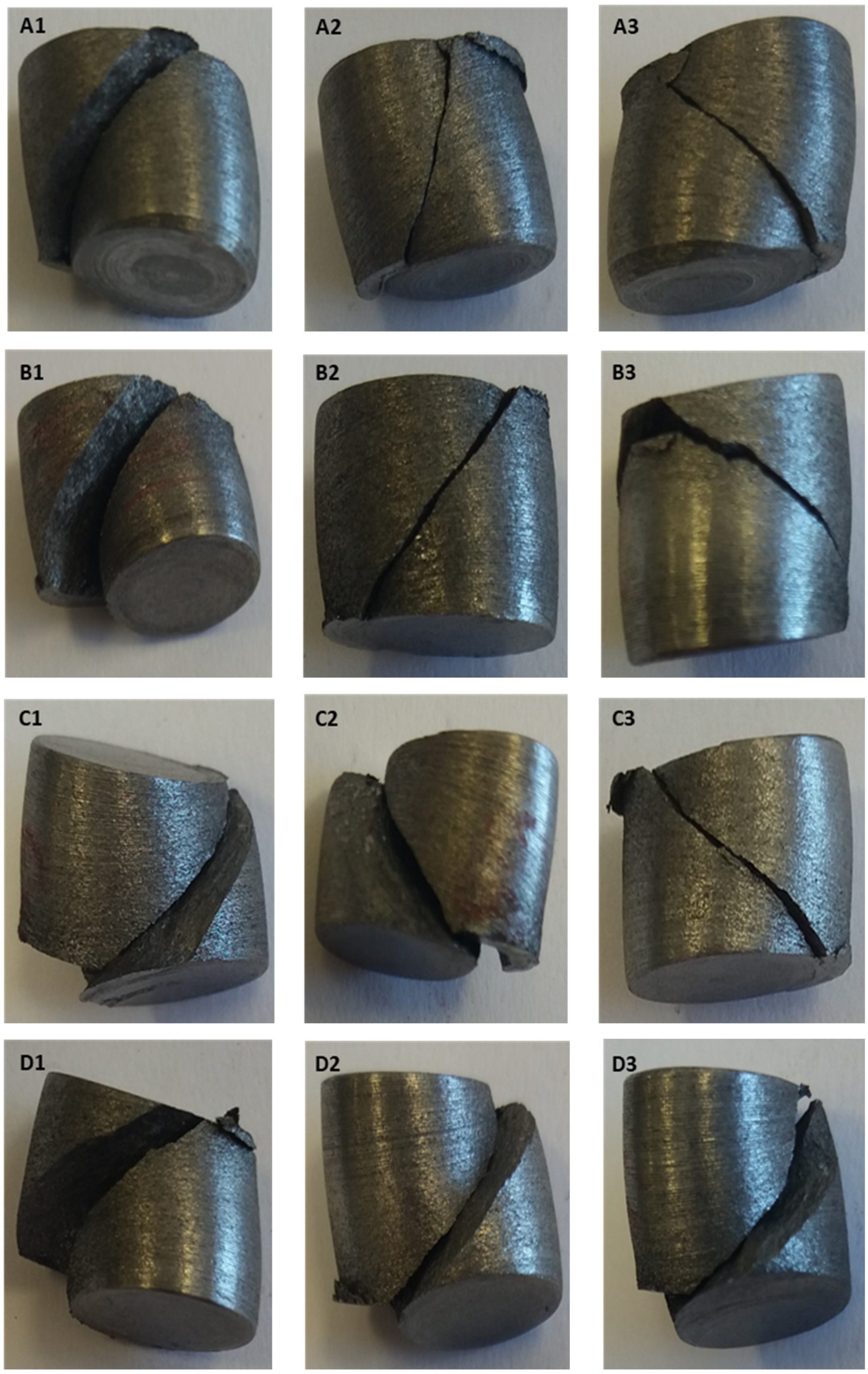

Figure 3. Appearance of compressive strength fracture damage. (**A**): 0% ZrB_2; (**B**): 0.227% ZrB_2; (**C**): 0.455% ZrB_2; (**D**): 1.364% ZrB_2. 1–3 respectively represent three samples with the same addition ratio of ZrB_2.

All tests were conducted under similar conditions to compare the samples during wear tests. Wear rate values, wear volume amount, and friction coefficient values which were obtained in the wear tests (Figure 5) were compared with the sample values at different ZrB_2 addition rates and the values of the control sample without addition.

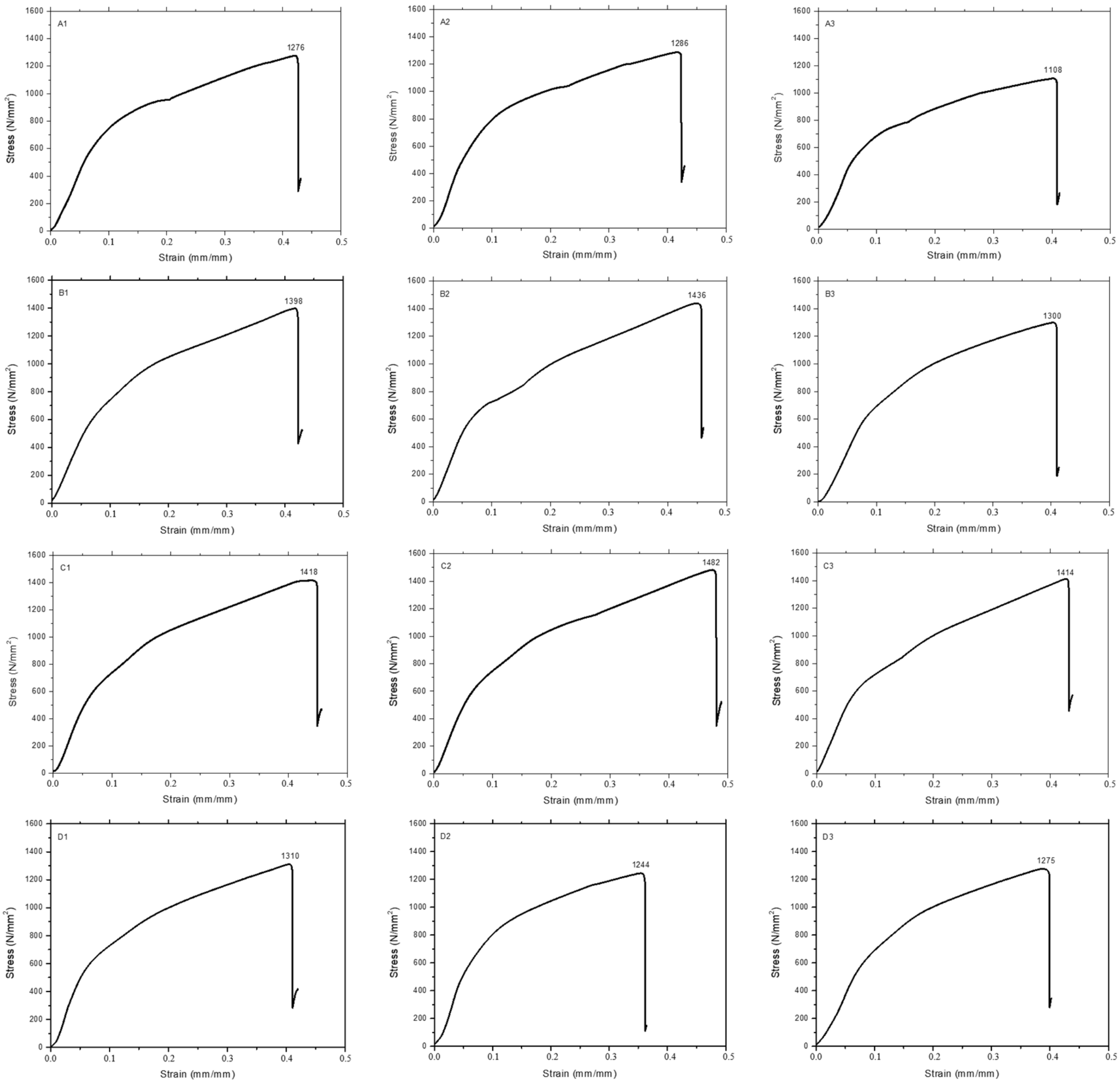

Figure 4. Compressive strength test stress–strain plots. (**A**): 0% ZrB_2; (**B**): 0.227% ZrB_2; (**C**): 0.455% ZrB_2; (**D**): 1.364% ZrB_2. 1–3 respectively represent three samples with the same addition ratio of ZrB_2.

(**a**) (**b**)

Figure 5. Wear test sample view (**a**,**b**).

Wear tests were performed on a Turkyus brand pin-on-disc wear device. When the load and addition rates applied in the tests were examined, the wear volume loss at the 5 N load value was found to be 0.1 mm^3 in samples B and D. The highest wear rate was observed in sample D at 5.2×10^{-5} mm^3/Nm. When the load value was 8 N, the highest wear volume loss was for sample B at 0.5 mm^3. The highest wear rate was detected as 13.1×10^{-5} mm^3/Nm in sample B. When the wear values at 10 N load value were examined, wear volume loss was highest in sample B, at 0.9 mm^3. The highest wear rate was observed in sample B at 18.8×10^{-5} mm^3/Nm. When the load value used in the wear test was 15 N, it was detected that the wear volume loss was highest in sample D at 2.4 mm^3. The highest wear rate was found in sample D at 31.6×10^{-5} mm^3/Nm. Wear resistance is generally inversely proportional to the wear volume of the material for a given set of test conditions in terms of conventional engineering metals [33]. Sundström et al. [34] determined that steel wear tended to decrease with increasing steel hardness. They also discovered that the wear resistance of steel depends on the microstructure and chemical composition. Steel with a similar microstructure indicates a linear decrease in weight loss with decreasing grain size and increasing carbon content. In this study's wear tests (Table 2), the general expectation was that when the load was kept constant, as the addition of ZrB_2 increased, the hardness values would increase and the particles that break off from the sample would decrease.

Table 2. Volume loss, wear rate, and coefficient of friction values of the samples.

Sample	Load (N)	Volume Loss (mm^3)	Wear Rate ($\times 10^{-5}$ mm^3/Nm)	Coefficient of Friction (COF)
A (0% ZrB_2)	5	0.0	1.4	0.96
B (0.227% ZrB_2)	5	0.1	3.2	0.61
C (0.455% ZrB_2)	5	0.0	0.7	0.39
D (1.364% ZrB_2)	5	0.1	5.2	0.42
A (0% ZrB_2)	8	0.1	2.4	0.61
B (0.227% ZrB_2)	8	0.5	13.1	0.53
C (0.455% ZrB_2)	8	0.3	8.2	0.40
D (1.364% ZrB_2)	8	0.4	8.8	0.42
A (0% ZrB_2)	10	0.1	1.6	0.53
B (0.227% ZrB_2)	10	0.9	18.8	0.48
C (0.455% ZrB_2)	10	0.7	13.4	0.37
D (1.364% ZrB_2)	10	0.6	11.4	0.35
A (0% ZrB_2)	15	0.1	1.9	0.51
B (0.227% ZrB_2)	15	1.8	23.8	0.34
C (0.455% ZrB_2)	15	0.9	12.3	0.38
D (1.364% ZrB_2)	15	2.4	31.6	0.36

When the friction coefficient changes of the samples (Table 2; Figure 6) were analysed, the friction coefficient value for the 5 N load was detected as 0.96 in sample A with the highest 0% ZrB_2 addition. The lowest friction coefficient value was 0.39 in sample C, with 0.455% ZrB_2 added. When the coefficient of friction for the 8 N load was examined, the highest value was found to be 0.61 in sample A with 0% ZrB_2 added. The lowest coefficient of friction was found to be 0.40 in sample C, with 0.455% ZrB_2 added. When the coefficient of friction for the 10 N load was examined, it was observed that the highest value was 0.53 in sample A with 0% ZrB_2 added. The lowest coefficient of friction was found to be 0.35 in sample D, with 1.364% ZrB_2 added. When the friction coefficient for the 15 N load was examined, the highest value was determined to be 0.51 in sample A with 0% ZrB_2 added. The lowest coefficient of friction was found to be 0.34 in sample B, with 0.227% ZrB_2 added. The comparison of the friction coefficients under the 5 N, 8 N, 10 N, and 15 N loads is illustrated in Figure 6. In his study, using the sand mould casting method, Gecü produced spheroidal graphite cast iron, which does not contain aluminium (Al) and contains 3% Al by weight. Samples kept in the austenite field at 900 °C for 90 min were rapidly cooled to

300 °C and kept at this temperature for 60 min after production. Wear tests of the produced samples were carried out in a dry environment using a ball-on-disc abrasion machine according to the ASTM G99-17 standard [30] . The experiments were abraded by Al_2O_3 balls at room temperature, at 40% relative humidity, with a sliding distance of 200 m, a sliding speed of 0.1 m/s, and a load of 10 N. While alloying with 3% Al increased the wear resistance, an austempering process yielded better results in the wear resistance of the unalloyed sample [35].

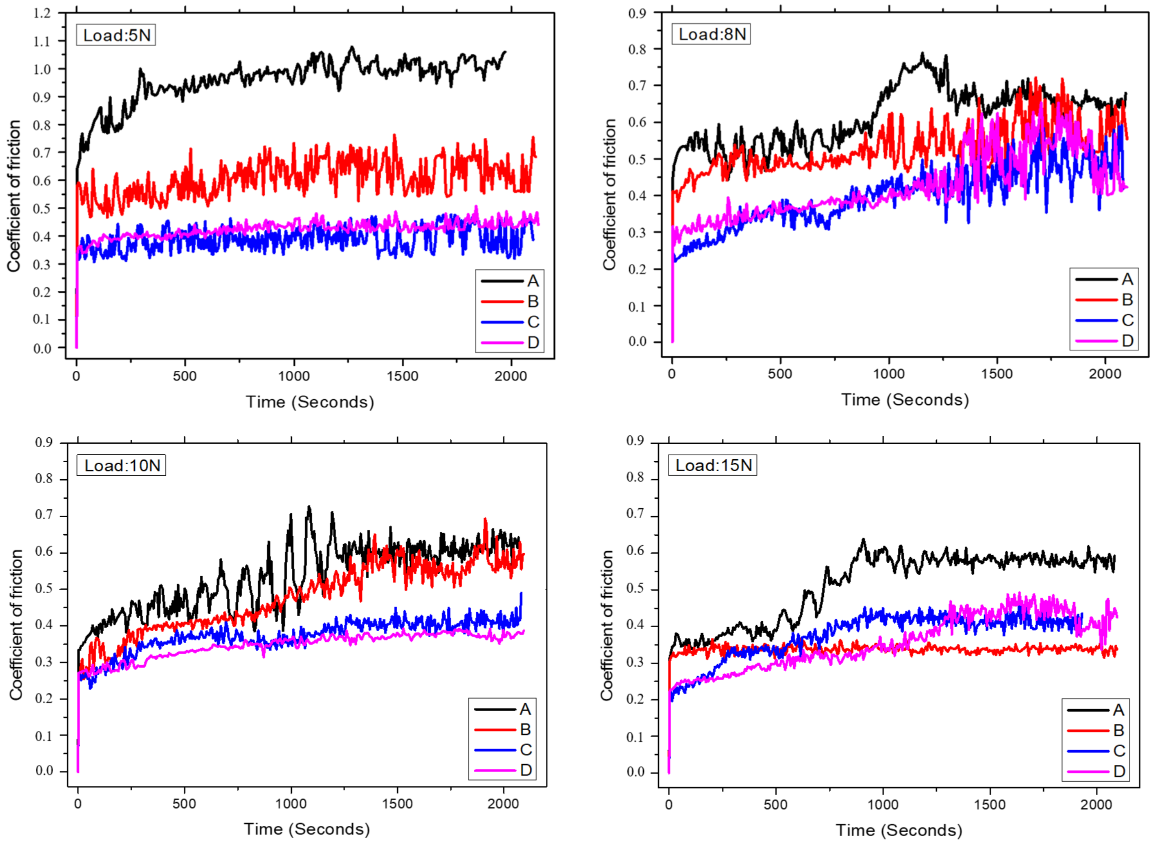

Figure 6. Comparison of friction coefficients under 5 N, 8 N, 10 N, and 15 N.

The worn surfaces of the samples were examined with a TESCAN MAIA3 XMU Scanning Electron Microscope (SEM) device, and wear mechanisms were determined. In sample A, it was observed that the wear volume loss increased with the increasing load. In this study, the highest wear occurred in particle ruptures and cavities in sample D, in which 1.364% ZrB_2 was added under a 15 N load. When the wear surfaces for the 5 N, 8 N, and 10 N loads were examined, wear was observed without particle breakage. Significant scratches were observed on wear surfaces parallel to the sliding direction. SEM microstructure views after wear are illustrated in Figure 7.

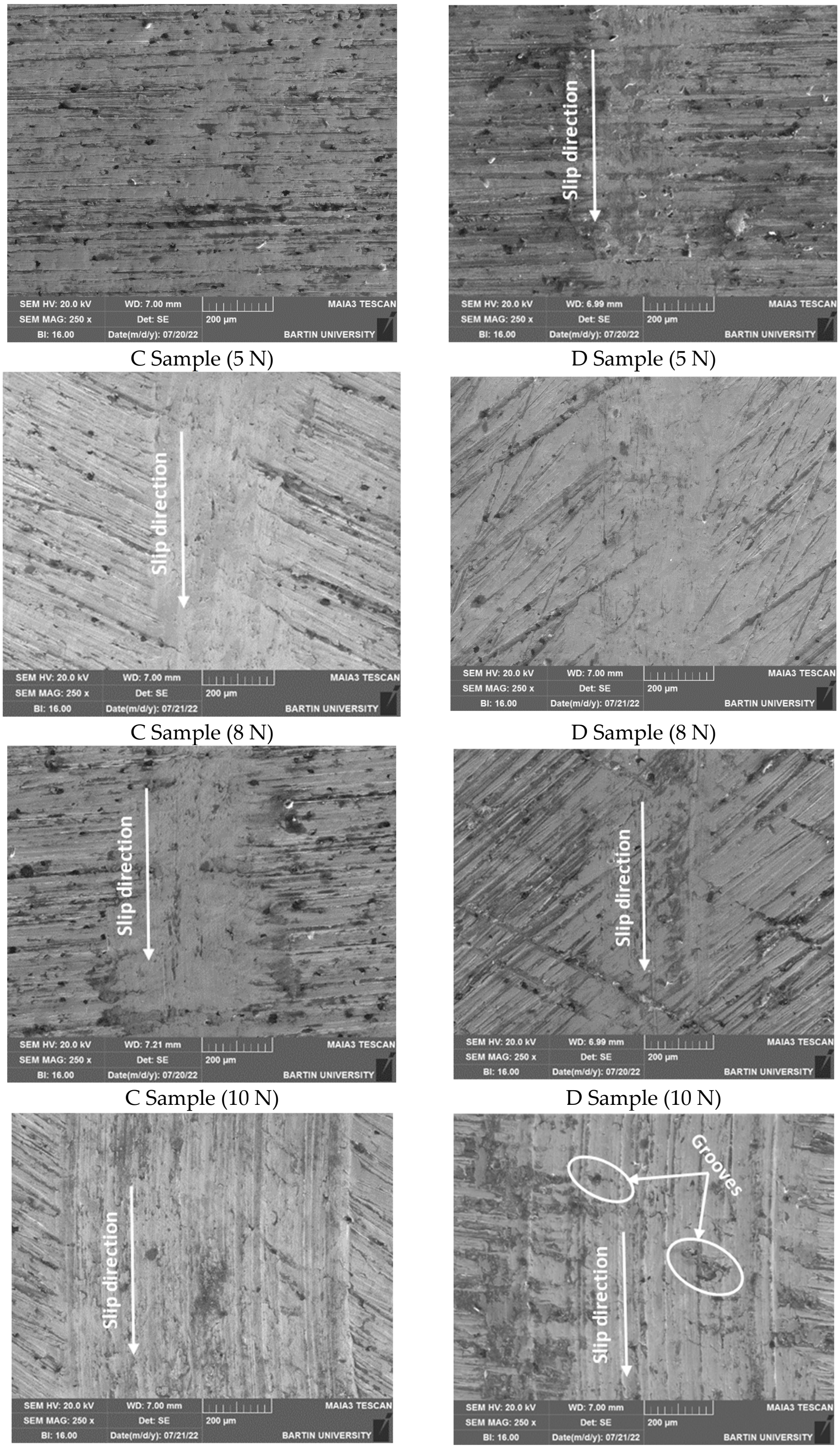

Figure 7. SEM images after wear tests.

4. Conclusions

Wear and gaps occur due to continuous operation of the ball and ball bearings on a steering gearbox. Increasing the strength values of steering gearbox bodies is necessary to prevent this wear. This study evaluated compression, hardness, and wear behaviour results by adding ZrB_2 at different rates for steering gearbox bodies made of spheroidal graphite cast iron. The results obtained in the study are presented below:

- In hardness measurement tests, the highest measurement was 243 HB in sample C. The closest value to this value was determined to be an average of 242 HB in sample D. When the results of the samples added at different rates were compared with the results of sample A, there was an increase in the hardness values.
- In compression tests, the highest value was detected as 1438 MPa in sample C. As the addition rate increased, it could be stated that there was an increase in the compressive stress values in general compared to sample A.
- When the wear condition was examined according to the increasing load values, it was observed that wear volume losses increased as the load value increased. Wear volumetric losses of sample B were detected as 0.1 mm^3 at the 5 N load, 0.5 mm^3 at the 8 N load, 0.9 mm^3 at the 10 N load, and 1.8 mm^3 at the 15 N load. A similar condition was observed in samples C and D.
- An increasing trend was observed in hardness values (sample A, 234 MPa; sample B, 239 MPa; sample C, 243 MPa; sample D, 242 MPa) with increasing additive ratios. Since it is difficult to remove particles from materials with increased hardness, the amount of wear decreases when hardness increases.

5. Future Research

Wear and gaps occur as the balls and ball bearings in steering gearboxes work under constant load. Such wear and gaps cause steering gearboxes to produce a lot of noise during operation. It is necessary to increase the strength of steering gearbox bodies to prevent these abrasions. In this study, the aim was to increase the strength values of steering gear box bodies composed of spheroidal graphite cast iron by adding zirconium diboride (ZrB_2) at different rates (sample A: 0%; sample B: 0.227%; sample C: 0.455%; and sample D: 1.364%). These produced samples' compressive strength, hardness, and wear resistance traits were investigated. A similar study for grey-cast iron could be conducted in following studies. The effects of ZrB_2 addition in different proportions to spheroidal graphite cast iron and grey cast iron on compression, hardness, and wear treatment might be compared and analysed.

Author Contributions: R.Y.: Conceptualization, methodology, visualisation; R.O.: resources, investigation; R.Y. and R.O.: writing—original draft preparation, writing—review and editing. All authors have read and agreed to the published version of the manuscript.

Funding: This research received no funding.

Institutional Review Board Statement: Not applicable.

Informed Consent Statement: Not applicable.

Data Availability Statement: All data generated and used in this study are included in the submitted manuscript.

Conflicts of Interest: The authors declare no conflict of interest.

References

1. Ceschini, L.; Campana, G.; Pagano, N.; Angelini, V. Effect of laser surface treatment on the dry sliding behaviour of the EN-GJS400-12 ductile cast iron. *Tribol. Int.* **2016**, *104*, 342–351. [CrossRef]
2. Orłowicz, A.W.; Trytek, A. Effect of rapid solidification on sliding wear of iron castings. *Wear* **2003**, *254*, 154–163. [CrossRef]
3. Günen, A.; Soylu, B.; Karakaş, Ö. Titanium carbide coating to improve surface characteristic, wear and corrosion resistance of spheroidal graphite cast irons. *Surf. Coat. Technol.* **2022**, *437*, 128280. [CrossRef]

4. Pegoraro, M.A.; Tenailleau, C.; Ebel, A.; Malard, B.; Lacaze, J. Spheroidal graphite coalescence during thermal cycling in the ferritic domain of a high-silicon cast iron studied by optical microscopy and X-ray computed tomography. *Mater. Today Commun.* **2020**, *25*, 101422. [CrossRef]
5. Çolak, M.; Arslan, İ.; Gavgalı, E. Solidification simulation of gray cast iron and comparision with real cast. *Eng. Sci.* **2018**, *13*, 280–290. [CrossRef]
6. Diószegi, A.; Svidró, P.; Elmquist, L.; Dugic, I. Defect formation mechanisms in lamellar graphite ıron related to the casting geometry. *Int. J. Cast Met. Res.* **2016**, *29*, 279–285. [CrossRef]
7. Park, Y.K.; Ha, K.; Bae, K.C.; Shin, K.Y.; Lee, K.Y.; Shim, D.; Lee, W. Mechanical properties and wear resistance of direct energy deposited Fe–12Mn–5Cr–1Ni-0.4C steel deposited on spheroidal graphite cast iron. *J. Mater. Res. Technol.* **2022**, *19*, 3484–3497. [CrossRef]
8. Abboud, J.H. Microstructure and erosion characteristic of nodular cast iron surface modified by tungsten inert gas. *Mater. Des.* **2012**, *35*, 677–684. [CrossRef]
9. Shamanian, M.; Abarghouie, S.M.; Pour, S.R. Effects of surface alloying on microstructure and wear behavior of ductile iron. *Mater. Des.* **2010**, *31*, 2760–2766. [CrossRef]
10. Sun, G.; Zhou, R.; Li, P.; Feng, A.; Zhang, Y. Laser surface alloying of C-B-W-Cr powders on nodular cast iron rolls. *Surf. Coat. Technol.* **2011**, *205*, 2747–2754. [CrossRef]
11. Nili-Ahmadabadi, M.; Shamloo, R. Control of austenitic transformation in ductile iron aided by calculation of Fe-C-Si-X phase boundaries. *J. Phase Equilibria* **2001**, *22*, 194–198. [CrossRef]
12. Zhang, Y.; Liu, F. Laser induced domino exfoliation of graphite to graphene in spheroidal graphite cast iron. *Surf. Coat. Technol.* **2016**, *285*, 235–241. [CrossRef]
13. Chen, X.-R.; Zhai, Q.-J.; Dong, H.; Dai, B.-H.; Mohrbacher, H. Molybdenum alloying in cast iron and steel. *Adv. Manuf.* **2019**, *8*, 3–14. [CrossRef]
14. Wang, Z.F.; Yao, M.; Zhang, X.B.; Wang, X.D. Optimization Control for Solidification Process of Secondary Cooling in Continuous Casting Steel. *Appl. Mech. Mater.* **2012**, *263–266*, 822–827. [CrossRef]
15. Triani, R.M.; Neto, J.B.T.D.R.; Oliveira, P.G.B.D.; Rêgo, G.C.; Neto, A.L.; Casteletti, L.C. In-Situ production of metal matrix composites layers by TIG surface alloying to improve wear resistance of ductile cast iron using a Buffer-Layer and post weld heat treatment. *Coatings* **2023**, *13*, 1137. [CrossRef]
16. Erturk, S.O.; Ozel, A. Investigation on the production of solution strenghted ductile iron part grade 500-14. *Bayburt Univ. J. Sci.* **2020**, *3*, 41–45.
17. Collini, L.; Pirondi, A. Microstructural, multilevel simulation of notch effect in ferritic ductile cast iron under low cycle fatigue. *Int. J. Fatigue* **2022**, *162*, 106993. [CrossRef]
18. Jost, B.; Klein, M.; Beck, T.; Eifler, D. Out-of-phase Tmf lifetime calculation of en-GJS-600 (ASTM 80-55-06) ductile cast iron based on strain increase tests and evaluation of cyclic deformation behavior in isothermal measuring intervals. *Int. J. Fatigue* **2018**, *117*, 274–282. [CrossRef]
19. Küçük, Y.; Altas, E.; Topcu, M.E. A comparative analysis of the effect of laser surface treatment on the dry sliding wear behavior of ductile cast irons with different microstructures. *Optik* **2023**, *274*, 170540. [CrossRef]
20. Wang, B.; Pan, Y.; Liu, Y.; Lyu, N.; Barber, G.C.; Wang, R.; Cui, W.; Qiu, F.; Hu, M. Effects of quench-tempering and laser hardening treatment on wear resistance of gray cast iron. *J. Mater. Res. Technol.* **2020**, *9*, 8163–8171. [CrossRef]
21. Ghasemi, R.; Elmquist, L. A study on graphite extrusion phenomenon under the sliding wear response of cast iron using microindentation and microscratch techniques. *Wear* **2014**, *320*, 120–126. [CrossRef]
22. Hase, A. Visualization of the tribological behavior of graphite in cast iron by in situ observations of sliding interfaces. *Tribol. Int.* **2019**, *138*, 40–46. [CrossRef]
23. Masuda, K.; Oguma, N.; Ishiguro, M.; Sakamoto, Y.; Ishihara, S. Sliding wear life and sliding wear mechanism of gray cast iron AISI NO.35B. *Wear* **2021**, *474–475*, 203870. [CrossRef]
24. Hurtado-Delgado, E.; Huerta-Larumbe, L.; Pérez, A.F.M.; Aguirre-Sánchez, Á. Microcracks reduction in laser hardened layers of ductile iron. *Coatings* **2021**, *11*, 368. [CrossRef]
25. Guterres, N.F.D.S.; Rusnaldy, R.; Widodo, A. Effect of chill plate thickness on surface hardening and dimensional accuracy of nodular cast iron gears manufactured by the Chill casting method. *Designs* **2023**, *7*, 56. [CrossRef]
26. Aguirre, T.G.; Lamm, B.; Cramer, C.L.; Mitchell, D.J. Zirconium-diboride silicon-carbide composites: A review. *Ceram. Int.* **2022**, *48*, 7344–7361. [CrossRef]
27. Sonber, J.; Suri, A. Synthesis and consolidation of zirconium diboride: Review. *Adv. Appl. Ceram.* **2011**, *110*, 321–334. [CrossRef]
28. Chamberlain, A.L.; Fahrenholtz, W.G. Reactive hot pressing of zirconium diboride. *J. Eur. Ceram. Soc.* **2009**, *29*, 3401–3408. [CrossRef]
29. Karadeniz, E.; Çolak, M.; Barutçu, F. Investigation of impact of amount and type of inoculants on microstructure and mechanical properties of GGG60 spheroidal graphite cast irons. *Niğde Ömer Halisdemir Univ. J. Eng. Sci.* **2017**, *6*, 275–282. [CrossRef]
30. Canbilen, A.E.; Ürküt, B.B. Determining the nodularity and sphericity of ductile cast ıron by using ımage processing methods. *Eur. J. Sci. Technol. Spec. Issue* **2020**, *5*, 60–64. [CrossRef]
31. Khalil-Allafi, J.; Amin-Ahmadi, B. Influence of mold preheating and silicon content on microstructure and casting properties of ductile iron in permanent mold. *J. Iron Steel Res. Int.* **2011**, *18*, 34–39. [CrossRef]

32. Shinde, V.D.; Ravi, B.; Narasimhan, K. Solidification behaviour and mechanical properties of ductile iron castings with varying thickness. *Int. J. Cast Met. Res.* **2012**, *25*, 364–373. [CrossRef]
33. Rupert, T.J.; Schuh, C.A. Sliding wear of nanocrystalline Ni–W: Structural evolution and the apparent breakdown of Archard scaling. *Acta Mater.* **2010**, *58*, 4137–4148. [CrossRef]
34. Sundström, A.; Rendón, J.; Olsson, M. Wear behaviour of some low alloyed steels under combined impact/abrasion contact conditions. *Wear* **2001**, *250*, 744–754. [CrossRef]
35. Gecü, R. Investigation of the effects of aluminum addition and austempering heat treatment on wear behavior of ductile cast irons. *Niğde Ömer Halisdemir Univ. J. Eng. Sci.* **2022**, *11*, 423–430. [CrossRef]